Supplementary Materials

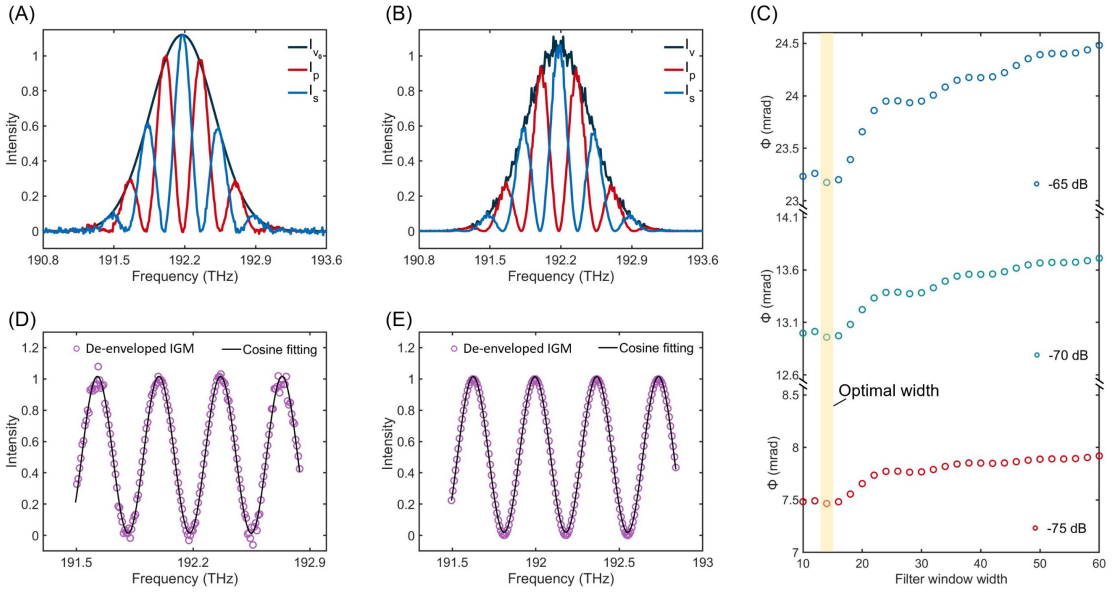

Fig. S1 Simulation results of the laser spectrum and orthogonally polarized IGMs with (A) intensity noise and (B) phase noise. (C) Phase resolution results obtained by applying the CPFT method with varying filter window widths to IGMs affected by phase noise levels of -65 dB, -70 dB, and -75 dB. (D) IGM with only intensity noise that have undergone PSD processing, along with the results of their cosine fitting. (E) IGM with only phase noise that have been processed with PSD and the resulting cosine fitting outcome.

The experimental process was simulated using MATLAB software. Initially, a time-domain window containing a Gaussian pulse with a width of 500 fs is constructed, with a size equal to the roundtrip time of the laser (45.05 ns), to represent the pulse in each cycle. The laser spectrum I_{v_0} was obtained by applying a Fourier transform to the pulse, as depicted by the dark green curve in Fig. S1(A). Different phase terms $e^{-i\omega t_1}$ and $e^{-i\omega t_2}$ are applied to the spectrum by the interferometer, where $\Delta t = t_1\text{-}t_2$ represents the time delay between the two interferometer arms. The modulus of the combined spectrum forms the interferogram (IGM) in dispersive spectral interferometry (DSI). Through this method, two IGMs with a π phase difference are established to represent the phase-shifted interferograms I_p and I_s.

The impact of intensity noise is simulated by adding a white Gaussian noise

matrix $N_{in}(n,\sigma^2)$ directly to the IGMs, as shown by the red and blue fringes in Fig. S1(A). Here, n denotes the data size of the IGM, and σ_{in}^2 characterizes the noise level. Intensity noise uniformly affects the amplitude of the IGMs without altering the initial spectrum.

Phase noise is introduced by applying a white Gaussian noise matrix $N_p(n,\sigma^2)$ to the time-domain window. This noise affected the initial spectrum by embedding different phase information before interference, as illustrated by the dark green curve in Fig. S1(B). Consequently, the interference fringes contained modulation information at different frequencies, as seen in the red and blue fringes in Fig. S1(B). It can be observed that phase noise influences the amplitude of the IGMs non-uniformly, correlating with fringe intensity.

In the phase retrieval process, the selection of the filter window width is generally considered to influence the overall level of phase noise, thereby affecting the phase results of real-time DSI obtained from FT and CPFT. To investigate this effect specifically, three sets of IGMs with different levels of phase noise are created, and the CPFT method is applied using various filter widths, with the results shown in Fig. S1(C). An optimal width is found in all three noise levels, indicated by the highlighted yellow section, which results in the best phase resolution. As the width increases, phase resolution degrades, explained by the retention of more phase noise in larger windows. The degradation of resolution is noise-level dependent, with a change of 1.3 mrad at -65 dB noise level as the width increases from 14 to 60, compared to only 0.5 mrad at -75 dB noise level. Moreover, a filter width smaller than

the optimal width can lead to the loss of interference information, also degrading resolution results. The optimal width is closely related to the signal peak width on the autocorrelation spectrum, influenced by pulse width and spectrum.

In real-time OPSI, a pair of IGMs with orthogonal polarization are used to remove the IGM's spectral envelope affected by phase noise. The processed IGM is represented by the purple circle in Fig. S1(e), showing fringes in a standard cosine function shape without any additional modulation information. The phase results can be obtained through cosine fitting (black curve). However, this de-envelope procedure is ineffective against intensity noise, as seen in Fig. S1(D), where the processed fringes are distorted by intensity noise, leading to increased uncertainty in the cosine fitting process, described as the noise-induced resolution limit.

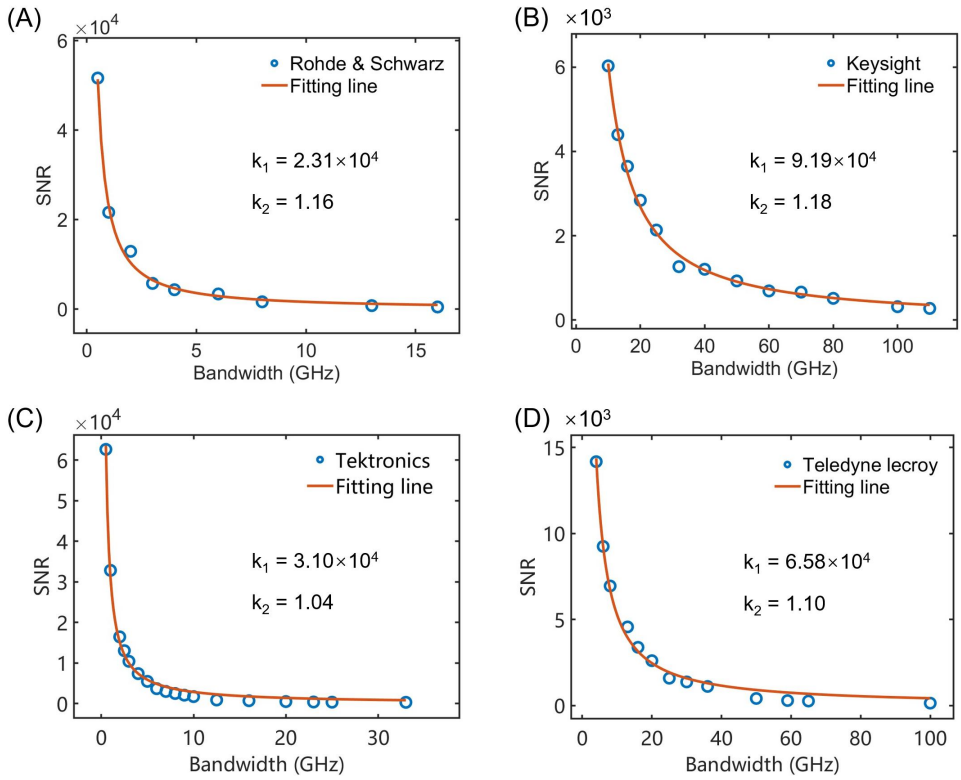

Fig. S2 SNR results corresponding to different sampling bandwidths, along with the fitting lines for oscilloscopes from four manufacturers: (A) Rohde & Schwarz ($k_1 = 2.31\times10^4$, $k_2 = 1.16$), (B) Keysight

($k_1 = 9.19\times10^4$, $k_2 = 1.18$), (C) Tektronics ($k_1 = 3.10\times10^4$, $k_2 = 1.04$), and (D) Teledyne LeCroy ($k_1 = 6.58\times10^4$, $k_2 = 1.10$).

When phase noise is eliminated, intensity noise becomes the sole factor affecting the SNR. Intensity noise primarily consists of shot noise, thermal noise, and amplifier noise, all of which increase proportionally with the sampling bandwidth. Although high-bandwidth detectors and oscilloscopes can capture more sample points, they result in a proportional decrease in SNR, meaning that phase resolution cannot be improved, as shown in Equation 9. Furthermore, quantization noise from the ADC and electrical noise from other components affect the SNR, creating an exponential relationship between bandwidth and SNR, described as $SNR=k_1/B^{k_2}$.

Using noise data from high-speed oscilloscopes from Rohde & Schwarz, Keysight, Tektronics, and Teledyne LeCroy, the relationship between sampling bandwidth and SNR was calculated, as shown in Fig. S2. Due to variations in electronic components and noise suppression techniques, different manufacturers have distinct values for k_1 and k_2. Oscilloscopes with larger k_1 values can achieve higher SNR at the same bandwidth; however, for all four oscilloscope types, $k_2>1$. According to Eq. (13), this implies that using higher bandwidth oscilloscopes can actually deteriorate phase resolution. This finding suggests that lower-bandwidth detectors could potentially improve resolution, providing guidance for the selection of equipment in real-time OPSI experiments.

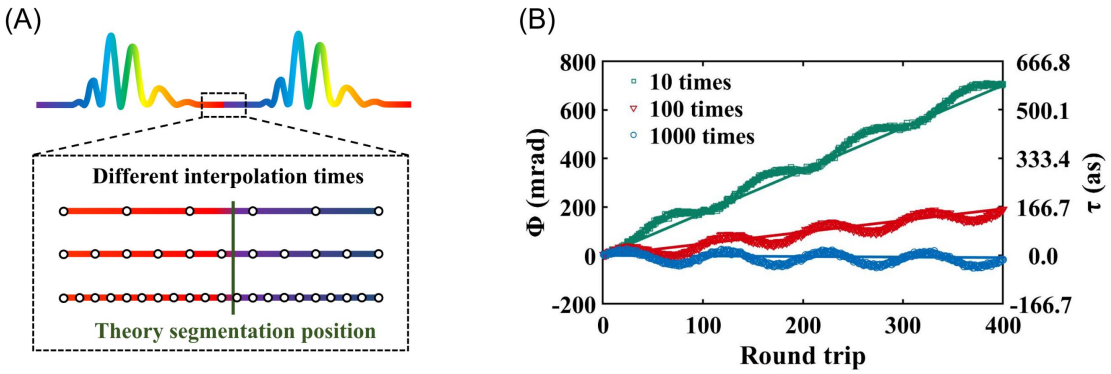

Fig. S3 | (A) Illustration of the influence caused by interpolation. (B) Evolution of phase retrieved by PSD-CF and theoretical calculation under different interpolation times.

In this section, we discuss the impact of the interpolation on the measurement results. The relative coordinate error between adjacent data points during segmentation can be reduced by increasing the interpolation factor. The principle is illustrated in Fig. S3(A), where white dots represent data points, and the green line indicates the theoretically perfect segmentation position—the position from which the interferograms, when segmented, align precisely with the center frequency. In practical terms, the segmentation position always incurs some error compared to the theoretical one, and this error linearly increases with the number of round-trips. This phenomenon is investigated using a 200, 50mV driving voltage under 10-, 100-, and 1000-times interpolation, as depicted in Fig. S3(B). Periodic phase modulation is observed with similar evolution and noise fluctuation, and the results more closely approximate the actual modulation signal with increased interpolation. The linear error can be mathematical calculated by $\Delta\varphi_\omega = \Delta\omega \cdot \tau$, where $\Delta\omega$ is the change in center frequency and the calculated lines match the evolution trend for the three cases in Fig. S3(B) (solid lines of the same color). The error accumulates to 700 mrad after 400 round-trips when the interpolation factor is only 10, but this value reduces to less than

5 mrad with an interpolation factor of 1000. However, further increasing the factor has a minimal effect on reducing the error, meanwhile a large amount of data can impede real-time fast measurements, requiring a trade-off. For measurements with short-term random variations, the detrend function can be directly applied to eliminate linear error.

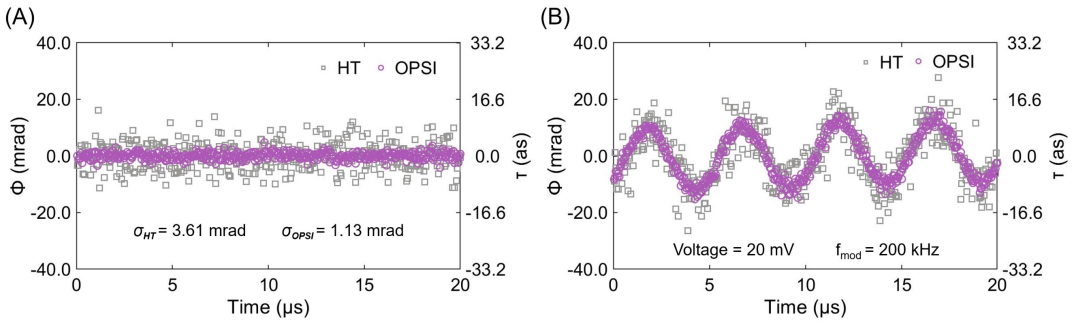

Fig. S4 (A) Phase retrieval results using Hilbert transform de-envelope and OPSI. (B) Evolutions of phase retrieved by Hilbert transform de-envelope and OPSI under a 200 kHz, 20 mV modulation signal

To make the comparison between our OPSI technique and the Hilbert transform (HT)-based de-envelope method, we retrieved phase evolution results using two different data processing methods under identical experimental conditions: a 3 ps time delay, 4 GHz sampling bandwidth, and varying phase modulation, as shown in Fig. S4. One method employed the HT-based de-envelope, while the other used the orthogonal polarization-based de-envelope, keeping all other steps unchanged. As shown in Fig. S4(A), it is evident that the OPSI technique (denoted by the purple circle) has a static resolution that is three times better than the HT-based method (denoted by the gray square), with respective resolutions of σ_{OPSI} = 1.13 mrad and σ_{HT} = 3.61 mrad. Furthermore, when a 200 kHz, 20 mV modulation signal was introduced to one arm of the interferometer, OPSI clearly resolved the modulation trend, whereas

the HT-based method produced a much less distinct result (as shown in Fig. S4(B)). These findings highlight the superior resolution capabilities of our OPSI technique compared to traditional de-envelope approaches such as the Hilbert transform.